Carbon 125 (2017) 132–138

Contents lists available at ScienceDirect

Carbon

journal homepage: www.elsevier.com/locate/carbon

Giant fullerene formation through thermal treatment of fullerene soot

Jacob W. Martin [a, b, *], Grant J. McIntosh [a], Rakesh Arul [a], Reece N. Oosterbeek [a], Markus Kraft [b], Tilo Söhnel [a, **]

[a] University of Auckland, School of Chemical Sciences, Symonds St, Auckland 1010, New Zealand
[b] University of Cambridge, Chemical Engineering & Biotechnology, Philippa Fawcett Drive, Cambridge CB3 0AS, UK

ARTICLE INFO

Article history:
Received 1 June 2017
Received in revised form
26 July 2017
Accepted 11 September 2017
Available online 13 September 2017

Keywords:
Giant fullerenes
Fullerene formation
Fullerene coalescence
Molecular cages
Nanoscale containers

ABSTRACT

Coalescence of fullerenes into giant fullerenes (C_n n > 100) has been observed in the gas phase and inside carbon nanotubes. In this work, we demonstrate the formation of giant fullerenes by heating fullerene soot. Extracting the majority of the magic number fullerenes (C_{60} and C_{70}) allowed the underlying distribution of fullerenes in the solid state to be measured. Upon heating at 800–1000 °C for 30–60 min under vacuum the mass distribution of fullerenes was found to shift toward larger masses. High resolution electron microscopy was used to compare formation of giant fullerenes by thermal heating and electron beam irradiation, showing the former produced more isolated giant fullerene fragments >1 nm in size. The driving force for coalescence and growth by thermal heating was suggested to be vertex strain at pentagonal sites, providing a route towards the synthesis of fullerenes up to C_{300}.

1. Introduction

Giant fullerenes have been observed in the earliest mass spectrometry studies of fullerenes. Yeretzian et al. [1] found that laser ablation of pure C_{60} powder in a stream of helium produced $(C_{60})_{n=2,3}$ adducts. These adducts were subsequently verified to be coalesced giant fullerenes and not simply aggregates by collision studies [2]. Preparation of dense clusters of C_{60} and bombardment with accelerated ions or pulses of light have found similar dimers and trimers, leading to an extended polymeric structure [3–8].

Coalescence of fullerenes has also been observed for the magic number fullerene C_{60} inside carbon nanotubes, under heating or electron beam irradiation, two C_{60} fullerenes or metallofullerenes will form dimers [9,10] and then an extended structure [11,12]. Coalescence of fullerenes and nanotubes have also been observed in several instances, such as the formation of nanobuds from nanotubes and fullerenes [13] and coalescence of nanotubes via electron beam radiation [14]. Fullerene coalescence in isolated crystals and soot has also been demonstrated using electron beam or neutron irradiation of fullerene soot [15,16]. However many of these products required localised sources of electron irradiation to form and were strongly polymerised.

Magic number fullerenes constitute locally stable cages and the process of coalescence is driven by a significant reduction in the free energy due to a decrease in the curvature of the pyramidalised carbons towards the graphene limit [17,18]. The production of the large numbers of C_{60}/C_{70} has been suggested to be due to the thermodynamically dissipative, far-from equilibrium systems in which they form. After formation of higher fullerenes the system loses [19] (and perhaps gains) [20] C_2 with magic number, symmetric fullerenes being produced due to their local reduced reactivity compared with their neighbor cages [21].

Unlike small symmetric fullerenes, which are only capable of holding 1–5 atoms, giant fullerenes could find applications as containers for larger molecules or collection of small molecules [22]. However, the controlled coalescence of small fullerenes into large single giant fullerenes has yet to be reported in the solid state.

We present a method to produce isolated giant fullerenes via thermal heating. By extracting C_{60} and C_{70} from fullerene soot we reveal the underlying structure of the giant fullerene distribution using laser desorption mass spectrometry. We then show that

Abbreviations: LDI-TOF MS, Laser desorption ionisation time of flight mass spectrometry; HRTEM, High resolution transmission electron microscopy; XPS, X-ray photoelectron spectroscopy; MALDI-TOF/TOF, Matrix Assisted Laser Desorption Ionisation Time of Flight/Time of Flight.

* Corresponding author. University of Cambridge, Chemical Engineering & Biotechnology, Philippa Fawcett Drive, Cambridge CB3 0AS, UK
** Corresponding author. University of Auckland, School of Chemical Sciences, Symonds St, Auckland 1010, New Zealand.
E-mail addresses: jwm50@cam.ac.uk (J.W. Martin), t.soehnel@auckland.ac.nz (T. Söhnel).

http://dx.doi.org/10.1016/j.carbon.2017.09.045
0008-6223/

heating leads to coalescence into giant fullerenes. The mechanism for formation and the extent to which fullerene size could be increased are discussed.

2. Materials and methods

Arc discharge fullerene soot was purchased from Sigma-Aldrich. Small fullerenes C_{60} and C_{70} were selectively extracted using boiling toluene via Soxhlet extraction for 48 h prior to heat treatment. Soot with C_{60} and C_{70} extracted was then placed in quartz tubes and heated in a tube furnace. During the reaction a dynamic vacuum of <0.1 Torr was applied to the reaction tube providing an environment that kept the carbon vapor at a minimum. After heating, the quartz was immediately quenched in water, which rapidly cooled the sample to room temperature.

2.1. Mass spectroscopy

An UltrafleXtreme Matrix Assisted Laser Desorption Ionisation Time of Flight/Time of Flight (MALDI-TOF/TOF) mass spectrometer was used for characterising the positive ions corresponding to the mass distribution of carbon fragments present in the solid-state fullerene samples. Ions were produced using a nanosecond pulsed 355 nm frequency tripled Nd:YAG laser (1 kHz repetition rate, ~5 ns pulse duration, maximum power of 2.3 μJ, spot size of 100 μm with a maximum laser fluence of 29.3 mJ/cm^2). The Bruker Peptide calibration standard was used for calibrating the instrument.

2.2. Transmission electron microscopy

Soot was imaged using a high resolution Tecnai FEG20 transmission electron microscope (HRTEM) with an accelerating voltage of 200 kV and an electron beam intensity of 300 A/cm^2. Soot was prepared by suspension in ethanol and deposited onto a holey carbon grid. The edges of the soot were imaged for fullerene fragments and their sizes were analysed as described previously [23]. For the electron beam irradiation experiments, unheated solvent extracted soot was used with an electron beam intensity of 3600 A/cm^2 to cause transformation of the material. A slow scan Ultrascan 1000 camera (Gatan, Pleasanton, CA, USA), was used to acquire pictures with 0.5 s exposures every 30 s over 20 min.

2.3. Simulations

Electronic structure calculations were performed with the CBS-QB3 [24] composite method in Gaussian 09, which provided accurate energies through extrapolation to the basis set limit [25]. Corannulene fragments were used to describe, as an initial approximation, the energetics of vertex strain in larger fullerenes. Redundant internal coordinates were used to constrain the dihedral angles around the central pentagon. The vertex strain energy per carbon atom for a given fullerene size was determined from these strained corannulene fragments, which were mapped onto a sphere using the pentagonal carbon atoms and the next nearest hexagonal carbons. Using the power law relationship found between the radius and carbon number in fullerenes [26], the radius of the sphere could be correlated with a fullerene size. Sizes ranged from C_{60} (with the smallest dihedral being 142°) to corannulene (dihedral 154°). Molecular dynamics simulations were performed using the LAMMPS software [27]. The CHO-2016 ReaxFF forcefield was employed, which has been recently parameterised for sp^2 carbon and combustion systems [28]. Low symmetry (C_2) fullerenes C_{62} and C_{82} were chosen from the Yoshida database [29] and placed one carbon bond length apart with oxygen in various positions described below. A Berendsen thermostat was employed to maintain a constant temperature of 2500 K and a time steps of 0.25 fs was used. Visual molecular dynamics program (VMD) was used for visualising the trajectory and a video is included in the supplementary information [30].

Supplementary video related to this article can be found at http://dx.doi.org/10.1016/j.carbon.2017.09.045.

3. Results

3.1. Distribution of fullerenes in the solid state

Care must be taken in analysing the mass spectrum of fullerenes from 3rd order Nd:YAG sources as the higher fullerenes are more readily desorbed than smaller fullerenes, which require a higher energy pulse such as a 9th order Nd:YAG laser [31]. This makes comparison between the magic number fullerenes and the distribution of higher fullerenes difficult and so we restrict our investigations to changes in these species separately. Another important consideration is the laser fluence required to desorb the higher fullerenes [32]. We explored this further in the Supplementary, section one, but briefly, we found a negligible effect of the laser shot number on the mas spectrum, indicating fresh material was being removed with each shot and incubation effects were minimal (Fig. S3). Changing the laser fluence we found two laser energy thresholds. The first >11.1 mJ/cm^3 provided sufficient energy to ionise the higher fullerenes. Increasing the laser power did not change the position and shape of the distribution until a second threshold was reached. This second threshold (>15 mJ/cm^3) produced small fragments from 0 to 300 *m/z* and caused a significant change and increase in the mass of the distribution (Figs. S2 and S4). These small fragments have been observed in the gas phase formation of fullerenes by Maul et al. [33]. Comparing fullerene soot with nanocrystalline graphite (Fig. S1) we find, for high laser fluence, similar low mass fragment ions, however we did not observe the C_2 separated log-normal mass distribution. Indicating that the conditions of laser vaporisation of carbon inside the mass spectrometer do not favour fullerene formation from small fragment ions and that, for the fullerene soot, the small fragments modify the already existing fullerene distribution.

Fig. 1 compares the as-produced fullerene soot with that of the toluene extracted fraction predominately made up of magic number fullerenes C_{60} and C_{70}. Coalescence products were clearly seen for the toluene extract (Fig. 1b) where fragments are seen around C_{60} and dimers and trimers are observed. For the unextracted soot (Fig. 1a) we find a distribution of higher fullerenes (C_n n > 70) and overlaid evidence of similar coalescence products found for the toluene extracted fraction of C_{60}/C_{70}. The laser power required to reach the threshold to see the distribution of higher fullerenes for Fig. 1 a) was above the second threshold (15.8 mJ/cm^3) which caused significant fragmentation of C_{60}/C_{70} producing adducts which formed dimers and trimers that obscured the underlying distribution of higher fullerenes. We suggest that due to the large number of C_{60}/C_{70} fullerenes in the soot compared to the higher fullerenes much of the laser power was absorbed by the magic number fullerenes leading to unwanted fragmentation and coalescence of the magic number fullerenes.

The selective extraction of C_{60} and C_{70} over higher fullerenes by toluene has been commented on earlier and suggested to be due to the large HOMO-LUMO gap in the magic number symmetric small fullerenes [34]. We used this method to remove a significant fraction of C_{60}/C_{70} from the soot, allowing the underlying distribution of higher fullerenes to be measured without fragmentation products (Fig. 2a). For the mass spectrum shown in Fig. 2 the laser power was set above the first and below the second threshold by

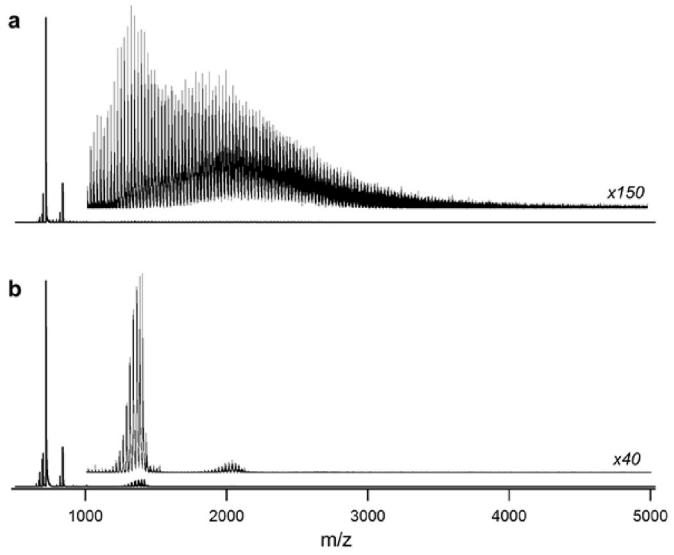

Fig. 1. LDI-TOF mass spectra of fullerene soot (500 shots 15.8 mJ/cm^3), a) unextracted soot (without C_{60}/C_{70} removal) and b) toluene soluble fraction of the fullerene soot showing extracted C_{60}/C_{70}. Insets from 900 to 3500 *m/z* show enlargements of 150 and 40 times respectively.

monitoring the region from 0 to 300 *m/z* to ensure no fragments were present which might alter the distribution. The mass spectra shows evidence that certain fullerenes in the range C_{60}–C_{84} have higher than expected populations due to their higher symmetry (Fig. 2a inset), which has been observed previously [4,35]. The comb distribution of higher fullerenes separated by C_2 (24 *m/z*), excluding the magic number fullerenes, was found to follow a log-normal size distribution ($\propto exp(-\log(x/x_0)/\sigma)$ with $x_0 = 1457$ *m/z* ~ C_{121}, $\sigma = 0.30$). This corroborates with the log-normal distribution of the size of giant fullerenes found previously in gas phase mass spectrometry [33] and HRTEM [23].

3.2. Temperature induced coalescence of fullerenes in the solid state

Heating the soot under vacuum led to a reduction in the ion intensity (10 times reduction) indicating a loss of species to the vacuum under elevated temperatures. We found for the remaining species a shift in the mass distribution towards the higher fullerenes (Fig. 2b–d), with the log-normal distribution fitting parameter x_0 increasing to C_{145}, C_{166} and C_{187} for an hour at 800, 900 and 1000 °C respectively. Considering the small magic number fullerenes, it can be seen that their concentrations are reduced as the distribution shifts towards the right.

From the mass spectrum of the higher fullerenes in Fig. 2 b, c and d we find the distribution of fullerenes shifted towards higher mass with isotope pattern suggesting integration of one, two or three oxygen into the fullerene structure with formula $C_{n-1}O$, C_nO_2 and C_nO_3 where n is an even number (see Fig. S7 in the supplementary information). Exposure of fullerenes to air is known to lead to integration of chemisorbed oxygen gas into the cage [36,37]. Using XPS we find that epoxides are the main oxygen species in the unheated and heated sample, however there was a reduction in the number of epoxides in favor of carbonyls in the heated samples (C–O:C=O decreases from 5:1 to 2.6:1) (see Fig. S6 in the supplementary information).

Fig. 3 a, b and c shows HRTEM images of the fullerene soot at low electron dose. Small circular fringe structures are observed near the edge of the soot particles which Goel et al. identified as fullerenes [23]. In the unheated sample fragments the size of C_{60} fullerene,

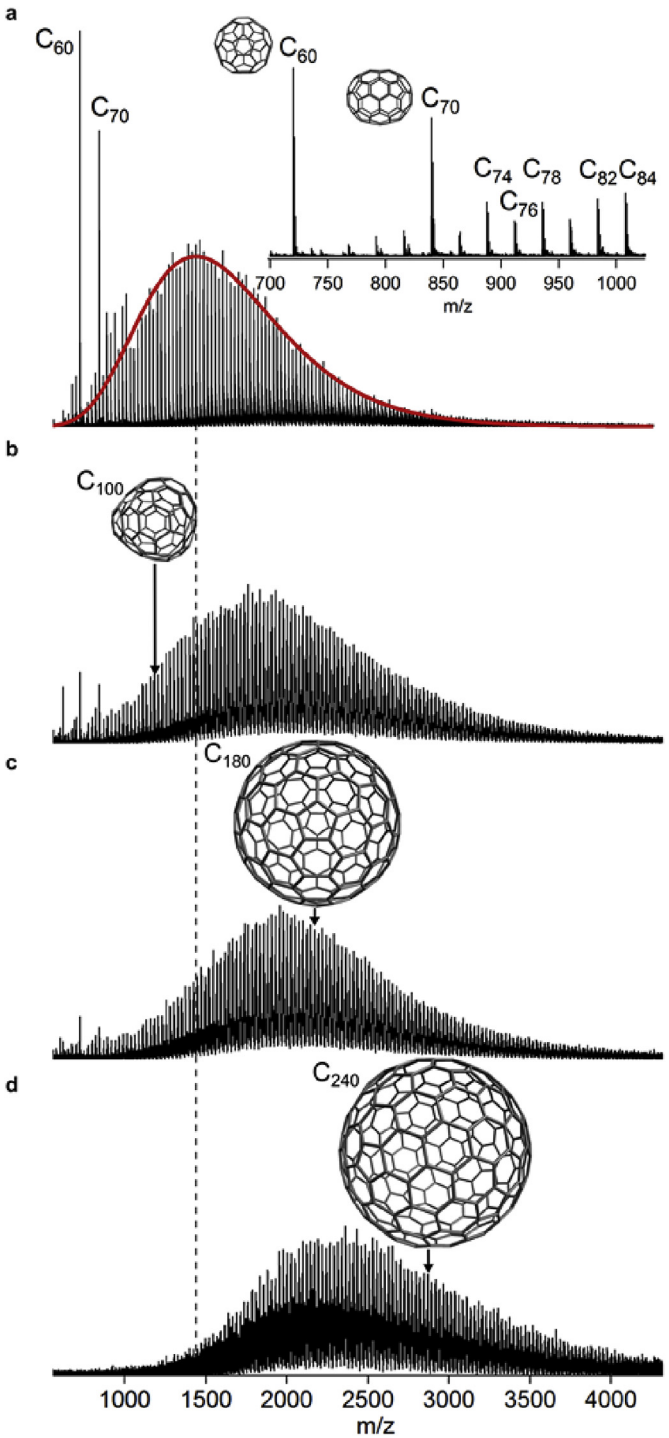

Fig. 2. LDI-TOF mass spectrum of fullerene soot after toluene extraction (500 shots 11–14 mJ/cm^3), a) Fullerene soot after Soxhlet extraction with toluene to remove most of the C_{60}/C_{70}. Magic number fullerenes are known to be relatively stable due to symmetry (C_{60}, C_{70}, C_{74}, C_{76}, C_{82} and C_{84}) see inset. Mass spectra of heated treated refluxed soot, 800 b), 900 c) and 1000 °C d) with heating for 1 h. The dashed line highlights the shift in the population towards greater mass. (A colour version of this figure can be viewed online.)

~0.7 nm in size, are observed which upon heating increase in size to 1.1–1.4 nm for the sample heated to 1000 °C for an hour. Comparing a collection of fullerenes from each sample we find the suggested size of the fullerenes from size analysis to align with the mass spectrum of those samples (see supplementary information). Goel

et al. also found that the size distribution of fullerene species followed the log-normal mass distribution [23]. Some elongated fringes are also produced, highlighted by arrows in Fig. 3 b and c, which indicate coalesced products.

3.3. Electron induced coalescence of fullerenes

In order to compare the thermal method of giant fullerene synthesis and electron beam irradiation, a sample of fullerene soot with the magic number fullerenes extracted was imaged under a high electron beam irradiation flux (Fig. 4). Within the first minute all of the small fragments <1 nm were consumed. After 11 min, a fullerene cage was observed to attach to a larger cage (as indicated by a black arrow starting Fig. 4c). Over the following 9 min this small fragment integrated into the larger structure and decreased its curvature. Graphitic structures indicated by extended long fringes were also found to form and overall a more connected and polymerised structure was observed. The electron irradiation is known to provide high energy conditions due to ionisation events and atom ejection induced by the electron beam [38]. But unlike ion induced coalescence where atom ejection leads to the formation of dumbbell-like agglomerates of magic number fullerene [5,8], electron irradiation provides significant heating to the sample allowing annealing of the structure to a greater degree than what was seen for the thermally treated soot. This shows in-situ the tendency of the structure to reduce its curvature through what appear to be coalescence reactions. Electron bombardment was found to form extended polymerised structure with no evidence of well-defined closed fullerenes as are observed in heated samples.

4. Discussion

We suggest that the thermal treatment allows fullerenes to coalesce on the surface of the fullerene soot. The mass distribution shows a reduction in the magic number fullerenes C_{60} and C_{70} ,indicating they are consumed, in addition to a progressive increase in the peak of the mass distribution. The observation of large circular fringes in the electron micrographs indicates the formation of isolated giant fullerenes. However, the role of oxygen, the driving force for the coalescence and whether the giant fullerenes can be extracted requires further discussion.

Odd numbered fullerene fragments such as $C_{n-1}O$ indicate integration of oxygen through the loss of carbon monoxide ($C_n + O_2 \rightarrow C_{n-1}O + CO$). Epoxidation of magic number fullerenes leads to stable cages for a few integrated oxygens and then cage opening for three or more oxygens in various conditions [39]. Fullerenes attached to the end of carbon nanocones have been suggested to be joined by oxygen through a 2 + 2 cycloaddition reaction of an epoxide and a pentagonal ring [40]. Oxygen could be an important species anchoring the fullerenes to the fullerene soot. As a preliminary exploration of the role of oxygen in the coalescence, we conducted reactive forcefield simulations using the ReaxFF forcefield. The forcefield has been parameterised for sp^2 carbon and compared well with the quantum chemical DFTB method for fullerene formation [41]. A recent parameterisation of the forcefield (CHO-2016) has significantly improved the treatment of oxygen [28].

The first simulation consisted of oxygen reacting with the low symmetry C_{62} fullerene at elevated temperature (2500 K). Oxygen rapidly broke the pentagonal C–C bond forming two carbonyl groups. Interconversion to the epoxide then led to loss of carbon monoxide after 90 ps. This followed the reaction methods proposed for C_{60} ozonation but with the loss of CO as opposed to carbon dioxide [42].

At high temperatures the carbonyl interconverts to the epoxide radical (Fig. 5 v) with the later allowing for reaction with other cages. In the second molecular dynamics simulation we use this bonded C_{82} and $C_{61}O$ dimer and observe coalescence over 2.5 ns (Fig. 5c initial geometry). The carbonyl oxygen was found to be the more predominant species during coalescence. This matches electronic structure calculations for the odd numbered $C_{59}O$ - finding the carbonyl to be more stable than the epoxide [43]. The increase in the carbonyl fraction for the heated soot seen in the XPS further suggests heating integrates oxygen as protruding carbonyl structures. The coalescence occurs rapidly due to the initial bridged structure. The dominant transformation seen was a rotation of C_2 by 90° (Stones-Wales transformations) which was the main mechanism found for non-oxidised carbon cages [44]. The change from a peapod structure to a spherical structure is known to take on the order of microseconds as the Stones-Wales transformation has a high energy barrier [45]. Observation of elongated fullerenes structures in the electron microscopy of heated soot suggest that these oxidised fullerenes can coalescence into closed structures. Further work is needed to understand the many possible ways oxygen can be integrated into fullerenes and whether oxygen can catalyse the coalescence as has been found in mass spectrometry [46].

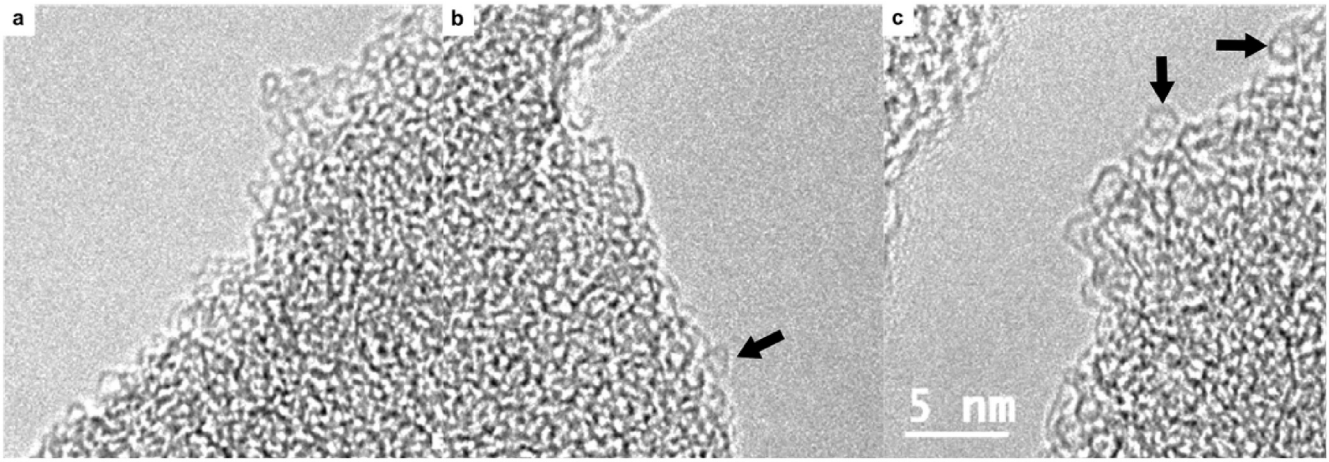

Fig. 3. Electron micrographs of fullerene soot after toluene extraction at the edge of soot particles. a) Small completely closed fullerenes are seen ~0.7 nm in size. Heating for b) 30 min at 800 °C and c) 1 h at 1000 °C led to increases in the fullerene size two with arrows being 1.15 nm and 1.36 nm along their longest axis. There is also an asymmetry to these fragments indicating fusion of two fullerenes into an elongated giant fullerene (see arrows). All images were taken at the same scale.

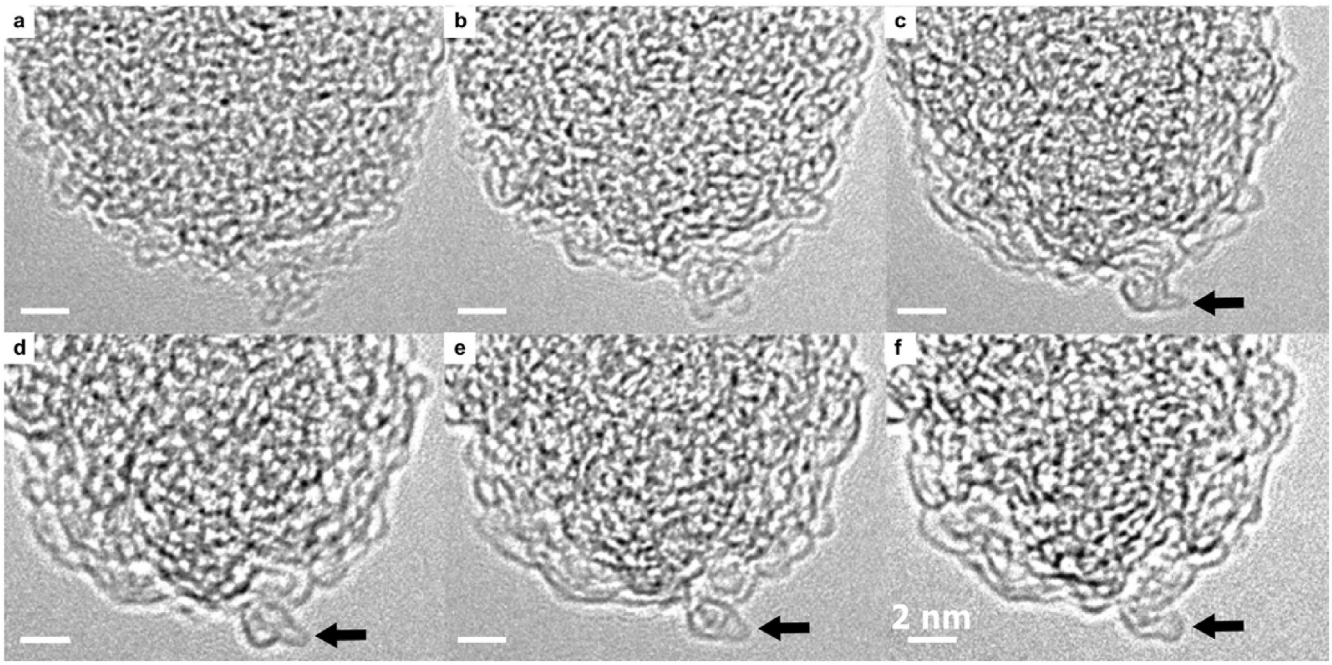

Fig. 4. Electron micrographs of unheated fullerene soot after toluene extraction (without C_{60}/C_{70}) under electron beam irradiation (3600 A/cm^2) for 0, 1, 11, 14, 16 and 20 min a)-f) respectively. Scale same for a)-f) with scale bar 2 nm.

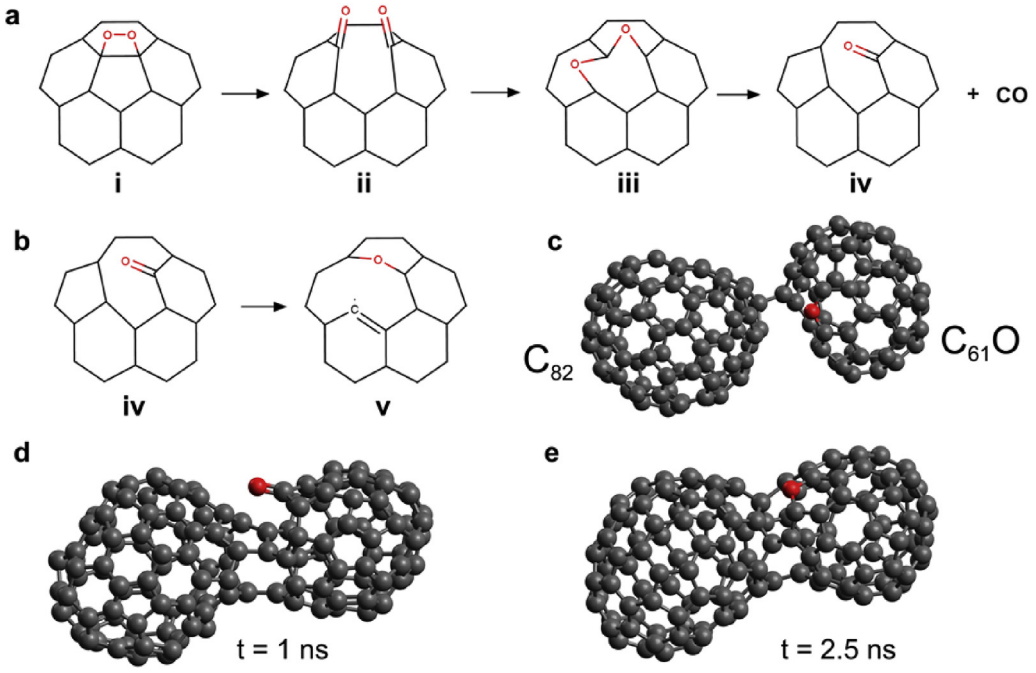

Fig. 5. Reactive molecular dynamic simulations a) Oxygen integration into fullerene structure. b) Upon heating the structure it was found to open and form an epoxide bridge leading to a reactive carbon radical. c) Initial geometry for the coalescence of the C_{82} and $C_{61}O$ dimer. Intermediates with carbonyl structures were found d) and integration of oxygen in epoxide structures was also observed e). (A colour version of this figure can be viewed online.)

As the coalescence dynamics observed are similar to non-oxidised fullerenes proceeding through C_2 rotation with the oxygen not taking a primary role in the coalescence we consider the driving energy for the coalescence to be due to reducing strain in the carbon lattice. It is well known that the pentagon site is the most reactive and often the site of initial cage opening in nanotubes [47], with a link found between reactivity and strain for small fullerene bowls (buckybowls) [48]. In the case of coalescence, the breaking of the pentagon C–C bond is the crucial step in allowing fullerenes to coalesce. In order to study the impact of strain on the reactivity of the pentagon carbon atoms the buckybowl corannulene was chosen. Corannulene is the simplest curved aromatic structure with a single pentagonal ring surrounded by five hexagonal rings. The internal strain of corannulene can be measured by

the angle it deflects from a planar trigonal sp^2 carbon, the pyramidalisation angle, which for corannulene is $\theta_P = 8.2°$ increasing to $\theta_P = 11.6°$ for C_{60} [18]. As the reaction class is the same and only the strain is varied we suggest the Bell-Evans-Polanyi principle can be applied where the activation energy trends for the bond breaking may be estimated from the reaction enthalpies with this initial bond breaking allowing a comparison of reactivity between fullerene cages. We calculated the change in energy as a function of the pyramidialisation angle by scanning the dihedral angles as a constrained redundant coordinate (varied between 142° and 154°). Then, by mapping this to the curvature of the (assumed) spherical corresponding fullerene, we were able to determine the increased energy due to the strain at the pentagon site (see supplementary information for further details). The energy of the corannulene fragment was found to increase considerably (40 kJ mol^{-1}), during constraining of the pentagon (Fig. 6). With an inset showing the delocalised π-bonding, molecular orbital. With increasing pyramidalisation there was a decrease in the electron density of π-bonding network as the carbon bonds take on more of a sp^3 character.

To determine whether the vertex strain could account for the size of fullerenes observed we developed a kinetic model to describe the gas phase dimerisation observed in Fig. 1b. For full details of the kinetic model see the supplementary information, but briefly we assume the reaction proceeds with second order kinetics, that is, first order in both reactants in a coalescing pair. The size dependent rate constant of coalescence was determined from the change in vertex strain energy $\Delta_R H$, which we propose is linearly related with the activation energy E_a for coalescence according to the Bell-Evans-Polanyi principle as the reactions are all of the same class but with varying degrees of vertex strain ($E_a = \alpha\Delta_R H + \beta$, $\alpha = 0.8$ *and* $\beta = 230$ kJ/mol). For simplicity, pre-exponential factors are assumed constant and identical (being 10^{-9} $L\,mol^{-1}\,s^{-1}$). Coalescence of C_{60} with some fragmentation products was used as a model system (Fig. 7b red). Comparing the simulated products (Fig. 7b black) and the products formed in the mass spectrometer (Fig. 7a black) there was qualitative agreement with the formation of coalescence products at $[C_{60}]_n$ n = 2,3,4 in decreasing intensity. Differences include the reduced amount of C_{120} which suggests C_{60} is less likely to coalescence due to its locally low potential energy - due to symmetry. Also fragmentation can be observed in the mass spectrum (left skew to the mass distribution) which is a result of C_2 loss which was not considered in the model. For the gas phase it appears that the reactivity of these small cages can be correlated with their reduced aromaticity due to strain and that fullerenes can be rapidly coalesced to produce fullerenes up to $C_{250\text{-}300}$ and during rapid heating of fullerenes in the solid state a similar range of fullerenes can be attained. Future work will be done on developing a model for coalescence in the solid state where the binary reaction approximation is invalid.

In terms of extraction, higher fullerenes (C_n n > 70) have only recently been extracted from soot in large quantities using electrochemical [34] and chemical [49,50] methods. This has allowed the extraction of gram scale quantities of higher fullerenes using redox methods [49]. These methods could potentially be explored for extraction of the oxygen crosslinked fullerenes.

Another possible approach could be to change the conditions under which fullerenes are formed. The energetics suggest that by increasing the temperature and residence time in the plasma the amount of giant fullerenes could be greatly increased without requiring initiation by oxygen or other impurities. This might enable a technique for the preparation of unoxidised giant fullerenes using current production methods for fullerene soot.

Comparing the internal volume of C_{260} to C_{60}, using the Van der

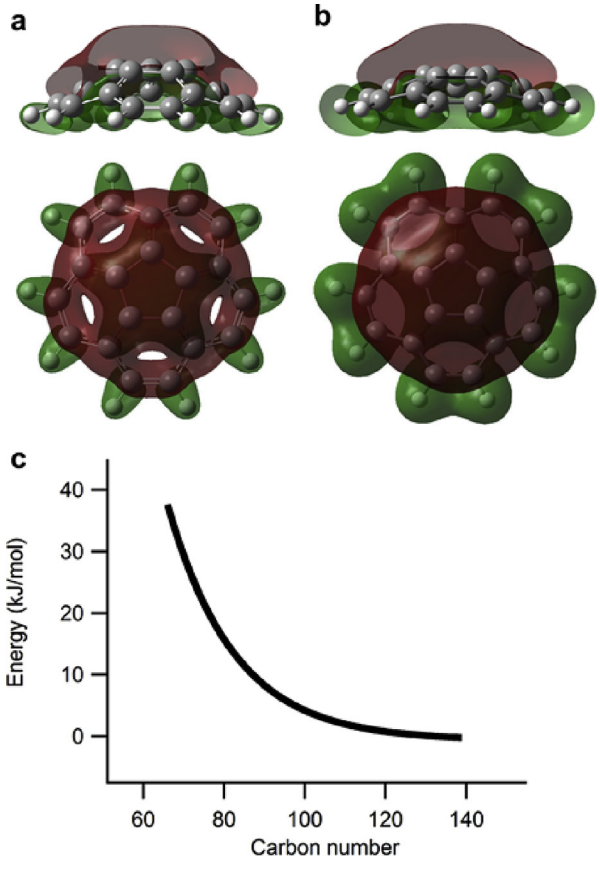

Fig. 6. Geometry and molecular orbital for strained corannulene with dihedral angles a) 142° and b) 154°. The delocalised π molecular orbital HOMO-21 (B3LYP 3-21G, 0.02 isovalue) is plotted as a cut plane through half of the geometry and from the top without the cut plane for the a) strained and b) unstrained structures showing the reduction in delocalisation of the π bonding. c) CBS-QB3 energy per carbon atom as a function of carbon fullerene number for a strained corannulene fragment mapped to a fullerene size. (A colour version of this figure can be viewed online.)

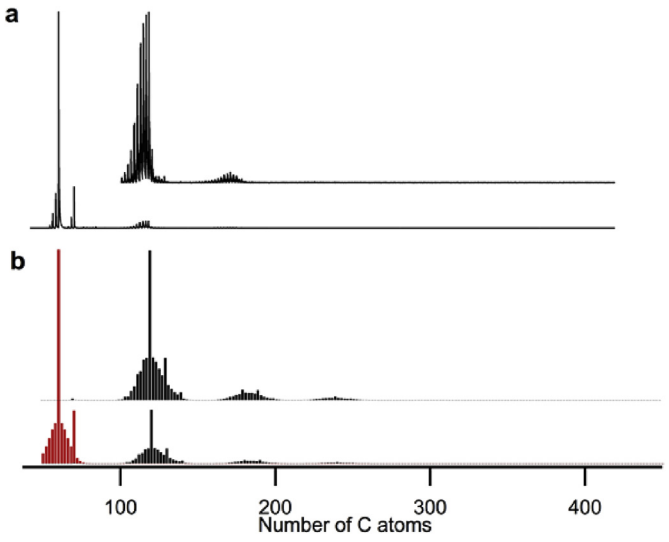

Fig. 7. a) LDI-TOF mass spectrum of C_{60} soot at maximum laser fluence showing C_{60} and C_{70} being the predominant species but also fragmentation products to the left of these fullerenes. The enlarged inset shows coalescence products corresponding to $(C_{60/70})_{2,3}$. b) The bottom spectrum shows simulated coalescence mass spectrum with the initial distribution shown in red and the final distribution in black with a magnified inset of the final distribution. (A colour version of this figure can be viewed online.)

Waals radius of carbon to be 1.7 Å, we can calculate the internal volume of 665 $Å^3$ and 27 $Å^3$ respectively. This is an increase of 25 ×, which greatly expands what could be trapped within these structures. Due to the reduced strain in these giant fullerenes they are predicted to be aromatic and conductive, which suggests they could be used as nanoscale Faraday cages for molecular electronics [51].

5. Conclusion

Extraction of C_{60} and C_{70} from fullerene soot allows for the mass distribution of the higher fullerenes to be observed unobscured by the fragments and coalescence products of C_{60} and C_{70}. This revealed the underlying log-normal distribution of higher fullerenes. By heating the soot under vacuum we were able to show an increase in the size of the fullerene fragments in the solid state. LDI-TOF MS showed an increase in the average fullerene mass and HRTEM confirmed that these correspond to completely closed giant fullerenes. Reactive forcefield simulations were used to elucidate the integration of oxygen and the coalescence of two fullerenes (C_{82} and $C_{61}O$). Transmission electron microscopy with electron beam irradiation showed the tendencies of high curvature carbon structures to reduce their curvature via coalescence. The high internal strain is found to be due to reduced π delocalisation in small fullerenes. This vertex strain as a function of carbon cage size was determined from ab initio energy calculations on a constrained corannulene fragment. This provides insight into the role of coalescence in the formation of fullerenes, including how conditions can be optimised for small magic number or giant fullerenes. We anticipate that combining recent methods to extract giant fullerenes, with the ability to size these fullerenes, will enable many promising applications.

Funding sources

This project is supported by the National Research Foundation (NRF), Prime Minister's Office, Singapore under its Campus for Research Excellence and Technological Enterprise (CREATE) programme.

Acknowledgment

Firstly, kind thanks to Prof. Emer. Robert Curl (Rice University) for his helpful discussions concerning the experimental design and fullerene formation. Thanks to Dr Shanghai Wei (University of Auckland) for his help in collecting the TEM images. Thanks to Prof. Christian Hartinger (University of Auckland) for his contribution analysing the isotope patterns from the mass spectrum. Dr Angus Grey (University of Auckland) for his expertise with the LDI-TOF mass spectrometer. Thanks to Dr Colin Doyle for collecting the XPS spectra. We would also like to thank Prof. M. Cather Simpson and Nina Novikova (Photon Factory, University of Auckland) for their support and help with sample preparation.

Appendix A. Supplementary data

Supplementary data related to this article can be found at http://dx.doi.org/10.1016/j.carbon.2017.09.045.

References

[1] C. Yeretzian, K. Hansan, F. Diederich, R.L. Whetten, Nature 359 (1992) 44.
[2] C. Yeretzian, K. Hansen, F. Diederich, R.L. Whetten, Atoms, Mol. Clust. 304 (1993) 300.
[3] F. Seitz, H. Zettergren, P. Rousseau, Y. Wang, T. Chen, M. Gatchell, J.D. Alexander, M.H. Stockett, J. Rangama, J.Y. Chesnel, M. Capron, J.C. Poully, A. Domaracka, A. Méry, S. Maclot, V. Vizcaino, H.T. Schmidt, L. Adoui, M. Alcamí, A.G.G.M. Tielens, F. Martín, B.A. Huber, H. Cederquist, J. Chem. Phys. *139* (3) (2013).
[4] H. Zettergren, H.A.B. Johansson, H.T. Schmidt, J. Jensen, P. Hvelplund, S. Tomita, Y. Wang, F. Martín, M. Alcamí, B. Manil, L. Maunoury, B.A. Huber, H.J. Cederquist, Chem. Phys. 133 (10) (2010) 1.
[5] H. Zettergren, P. Rousseau, Y. Wang, F. Seitz, T. Chen, M. Gatchell, J.D. Alexander, M.H. Stockett, J. Rangama, J.Y. Chesnel, M. Capron, J.C. Poully, A. Domaracka, A. Méry, S. Maclot, H.T. Schmidt, L. Adoui, M. Alcamí, A.G.G.M. Tielens, F. Martín, B.A. Huber, H. Cederquist, Phys. Rev. Lett. 110 (18) (2013) 1.
[6] D. Nugawela, S.J. Stuart, J. Jakowski, in: Proceedings of the 2014 Annual Conference on Extreme Science and Engineering Discovery Environment - XSEDE '14, ACM Press, New York, New York, USA, 2014, pp. 1–8.
[7] M. Hedén, K. Hansen, E.E.B. Campbell, Phys. Rev. A - At. Mol. Opt. Phys. 71 (5) (2005) 1.
[8] M. Gatchell, H. Zettergren, J. Phys. B 49 (16) (2016) 162001.
[9] C. Bousige, S. Rols, E. Paineau, S. Rouzière, C. Mocuta, H. Kataura, P. Launois, EPL Europhys. Lett. 103 (6) (2013) 66002.
[10] L. Guan, K. Suenaga, T. Okazaki, Z. Shi, Z. Gu, S. Iijima, J. Am. Chem. Soc. 129 (29) (2007) 8954.
[11] E. Hernández, V. Meunier, B.W. Smith, R. Rurali, H. Terrones, M. Buongiorno Nardelli, M. Terrones, D.E. Luzzi, J.-C. Charlier, Nano Lett. 3 (8) (2003) 1037.
[12] C.S. Allen, Y. Ito, A.W. Robertson, H. Shinohara, J.H. Warner, ACS Nano 5 (12) (2011) 10084.
[13] R.J. Nicholls, J. Britton, S.S. Meysami, A. Koos, a; Grobert, N. Chem. Commun. 49 (93) (2013) 10956.
[14] M. Terrones, Science (80-.). 288 (5469) (2000) 1226.
[15] D. Ugarte, Nature 359 (6397) (1992) 707.
[16] Y. Zhao, Z. Chen, H. Yuan, X. Gao, L. Qu, Z. Chai, G. Xing, S. Yoshimoto, E. Tsutsumi, K. Itaya, J. Am. Chem. Soc. 126 (36) (2004) 11134.
[17] J. Guan, Z. Jin, Z. Zhu, C. Chuang, B.Y. Jin, D. Tomanek, Phys. Rev. B - Condens. Matter Mater. Phys. 90 (24) (2014) 1.
[18] Y. Noël, M. De La Pierre, C.M. Zicovich-Wilson, R. Orlando, R. Dovesi, Phys. Chem. Chem. Phys. 16 (26) (2014) 13390.
[19] S. Irle, G. Zheng, Z. Wang, K. Morokuma, J. Phys. Chem. B 110 (2006) 14531.
[20] P.W. Dunk, N.K. Kaiser, C.L. Hendrickson, J.P. Quinn, C.P. Ewels, Y. Nakanishi, Y. Sasaki, H. Shinohara, A.G. Marshall, H.W. Kroto, Nat. Commun. 3 (May) (2012) 855.
[21] R.F. Curl, M.K. Lee, G.E. Scuseria, J. Phys. Chem. A 112 (46) (2008) 11951.
[22] D.M. Rudkevich, Bull. Chem. Soc. Jpn. 75 (3) (2002) 393.
[23] A. Goel, J.B. Howard, J.B. Vander Sande, Carbon N. Y. 42 (10) (2004) 1907.
[24] J.A. Montgomery, M.J. Frisch, J.W. Ochterski, G.A. Petersson, J. Chem. Phys. 112 (15) (2000) 6532.
[25] M. J. Frisch, G.W. Trucks, H.B. Schlegel, G.E. Scuseria, M.A. Robb, J.R. Cheeseman, et al., Gaussian 09, Revision A.02.
[26] S. Itoh, P. Ordejón, D.A. Drabold, R.M. Martin, Phys. Rev. B 53 (1996) 2132.
[27] S. Plimpton, J. Comput. Phys. (March 1995) 1–19.
[28] C. Ashraf, A.C.T. van Duin, J. Phys. Chem. A 121 (5) (2017) 1051.
[29] M. Yoshida, E. Osawa, Bull. Chem. Soc. Jpn. (1995) 2073–2081.
[30] W. Humphrey, A. Dalke, K. Schulten, J. Mol. Graph. 14 (1996) 33.
[31] P.W. Dunk, H. Niwa, H. Shinohara, A.G. Marshall, H.W. Kroto, Mol. Phys. 113 (15–16) (2015) 2359.
[32] O. Šedo, M. Alberti, J. Janča, J. Havel, Carbon N. Y. 44 (5) (2006) 840.
[33] J. Maul, T. Berg, E. Marosits, G. Schönhense, G. Huber, Phys. Rev. B 74 (16) (2006) 1.
[34] J.M. Alford, M.D. Diener, Nature 393 (6686) (1998) 668.
[35] J.A. Zimmerman, J.R. Eyler, S.B.H. Bach, S.W. McElvany, J. Chem. Phys. 94 (5) (1991) 3556.
[36] M. Wohlers, H. Werner, T. Belz, T. Rühle, R. Schlögl, Mikrochim. Acta 125 (1–4) (1997) 401.
[37] K.M. Creegan, J.L. Robbins, W.K. Robbins, J.M. Millar, R.D. Sherwood, P.J. Tindall, D.M. Cox, J.P. McCauley, D.R. Jones, J. Am. Chem. Soc. 114 (3) (1992) 1103.
[38] F. Banhart, Philos. Trans. A. Math. Phys. Eng. Sci. 2004 (362) (1823) 2205.
[39] L. Gan, Chem. Rec. 15 (1) (2015) 189.
[40] I. Suarez-martinez, J. Mittal, H. Allouche, M. Pacheco, M. Monthioux, M. Razafinimanana, C.P. Ewels, Carbon N. Y. 54 (2013) 149.
[41] H.-J. Qian, A.C.T. van Duin, K. Morokuma, S. Irle, J. Chem. Theory Comput. 7 (7) (2011) 2040.
[42] R.C. Chapleski, J.R. Morris, D. Troya, Phys. Chem. Chem. Phys. 16 (13) (2014) 5977.
[43] H. Jiao, Z. Chen, A. Hirsch, W. Thiel, Phys. Chem. Chem. Phys. 4 (20) (2002) 4916.
[44] Y.-H. Kim, I.-H. Lee, K.J. Chang, S. Lee, Phys. Rev. Lett. 90 (6) (2003) 65501.
[45] F. Ding, B.I. Yakobson, J. Phys. Chem. Lett. 5 (17) (2014) 2922.
[46] R.D. Beck, C. Stoermer, C. Schulz, R. Michel, P. Weis, G. Brauchle, M.M. Kappes, J. Chem. Phys. 101 (4) (1994) 3243.
[47] P.M. Ajayan, T.W. Ebbesen, T. Ichihashi, S. Iijima, K. Tanigaki, H. Hiura, Nature 362 (6420) (1993) 522.
[48] H.Y. Cho, R.B.M. Ansems, L.T. Scott, Beilstein J. Org. Chem. 10 (2014) 956.
[49] J.W. Raebiger, J.M. Alford, R.D. Bolskar, M.D. Diener, Carbon N. Y. 49 (1) (2011) 37.
[50] F. Beer, A. Gügel, K. Martin, J. Räder, K. Müllen, J. Mater. Chem. 7 (8) (1997) 1327.
[51] P. Delaney, J.C. Greer, Appl. Phys. Lett. 84 (3) (2004) 431.